Microwave photocurrent from the edge states of InAs/GaInSb bilayers

Jie Zhang,[1,*] Tingxin Li,[1] Rui-Rui Du,[1,2,†] and Gerard Sullivan[3]

[1]*Department of Physics and Astronomy, Rice University, Houston, Texas 77251, USA*
[2]*International Center for Quantum Material, Peking University, Beijing 100871, China*
[3]*Teledyne Scientific and Imaging, Thousand Oaks, California 91630, USA*

We measure microwave photocurrent in devices made from InAs/GaInSb bilayers where both the insulating bulk state and conducting edge state were observed in the inverted-band regime, consistent with the theoretical prediction for a quantum spin Hall (QSH) insulator. It has been theoretically proposed that microwave photocurrent could be a unique probe in studying the properties of QSH edge states. To distinguish a possible photoresponse between a bulk state and helical edge state, we prepare a Hall bar and Corbino disk from the same wafer. Results show that the Corbino-disk samples have a negligible photocurrent in the bulk gap, while clear photocurrent signals from the Hall-bar samples are observed. This finding suggests that the photocurrent may carry information concerning the electronic properties of the edge states.

The helical edge states have attracted much attention because of their topological properties such as the robustness against backscattering due to spin-momentum locking, and the subsequent conductance quantization observed in low-temperature transport measurements [1–3]. Inverted InAs/GaSb double quantum wells (DQWs) [4–10] and InAs/GaInSb DQWs [11–13] have been demonstrated to be a favored platform to study the helical edge state properties. Due to the spatial overlap between the electron and hole wave functions, a hybridization gap is opened in the bulk and conducting edges emerge. By utilizing the front/back gates, the Fermi level in the device can be continuously tuned [4–13]. Application of strain in InAs/GaInSb DQWs increases the bulk hybridization gap [12,13], thus opening the possibility for studying helical edge states ranging from strongly interacting to weakly interacting regimes.

Terahertz (THz) and infrared (IR) [14,15] spectroscopies have been proven to be powerful tools to probe two-dimensional (2D) and 3D topological materials. Recently, the photovoltaic effect was used to study electron spin imbalance on the edges in HgTe QWs induced by a circular photogalvanic effect in unbiased devices by selectively exciting spins [15] or utilizing the chiral properties of quantum materials such as Weyl semimetals [16]. Here we report the observation of microwave (MW) photocurrent in a Hall bar made of strained-layer InAs/GaInSb DQWs. In contrast, such photocurrent is absent in a Corbino disk where the edge state is shunted by metal electrodes. Our work thus demonstrates that the photocurrent signal primarily stems from the edge states. We measure the frequency and temperature dependence of the photocurrent and find that the application of a magnetic field can increase the photocurrent near the charge neutral point (CNP). Our results suggest that the electromagnetic wave

response could be a viable experimental window probing the helical edge states in quantum spin Hall insulators.

The experiments have been carried out on strained-layer InAs/Ga$_{0.68}$In$_{0.32}$Sb DQWs grown by molecular beam epitaxy on a GaSb substrate. The electron-hole QWs have a respective well width of 8 nm and 4 nm [Fig. 1(a)]; wafer details can be found in [12,13]. The samples fabricated for this wafer have been systematically characterized and have shown properties, such as approximately quantized edge conductivity to $h/2e^2$ for sample size up to 5 μm and reduced conductivity under an in-plane magnetic field, that are consistent with weakly interacting helical edge states [13]. The present samples were fabricated from the same wafer following exactly the same processes, and therefore their dc transport properties were found to reproduce those presented in [13].

A typical Hall bar with a length of 75 μm and width of 25 μm is patterned using photolithography and wet-chemical etching, as shown in Fig. 1(d). Ohmic contacts are made by selectively etching the samples down to the InAs QW and depositing Ti/Au as electrodes without annealing. A back gate is used to tune the Fermi level in the device. The ability to reach the quantum spin Hall (QSH) phase without a front gate enables the MW to interact with the helical edge states. The sample is immersed in He^3 liquid in a cryostat with a base temperature of 300 mK and equipped with a superconducting magnetic coil up to 8 T. The MW is produced by an Anristu signal generator with a single frequency ω in the range 2–40 GHz and is transmitted via a semirigid coaxial cable with an antenna in the end. The magnetotransport is measured by a standard low-frequency (frequency f) lock-in amplifier which also provides the amplitude modulation of the MW wave. A constant dc current ($\sim$10 nA) is fed into the current leads of the Hall bar used to provide directional selection for the excited carriers. In order to rule out the possibility that the observed photocurrent comes from the bulk contribution, a Corbino sample is fabricated on the same wafer using the same procedures, as shown in Fig. 1(c). The dc transport
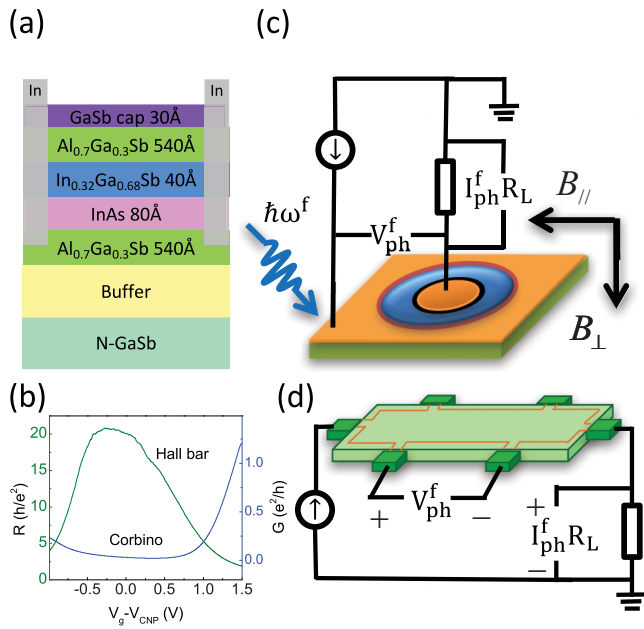
———————
*jz38@rice.edu
†rrd@rice.edu

FIG. 1. (a) Structure of strained-layer InAs/GaSb wafer used in the experiment, which hosts robust quantum spin Hall edge states. (b) Resistance measured for Hall-bar sample and conductance measured for the Corbino sample. (c) Experimental setup of the differential photovoltage V_{ph}^{f} and photocurrent I_{ph}^{f} measurement on a typical Corbino disk with MW amplitude modulation provided by locked-in amplifier frequency f. (d) Photoresponse measurement setup on a Hall-bar sample fabricated the same way as the Corbino sample shown in (c).
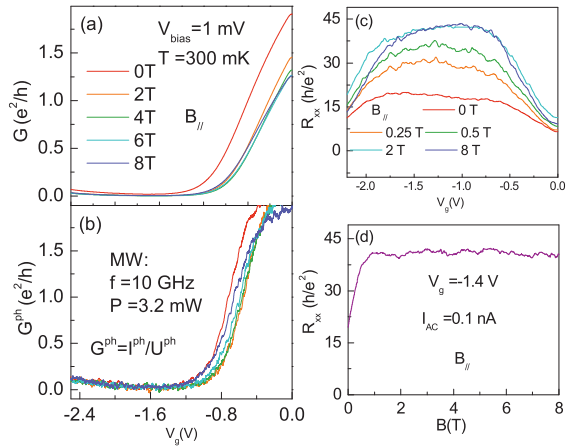

FIG. 2. (a) Magnetoconductance measurement of the insulating bulk state on a Corbino disk with a strong external parallel magnetic field (up to 8 T). 2D bulk is accessed, sweeping the backgate voltage, which indicates a completely insulating behavior, giving no evidence of gap closing at increasing magnetic field. (b) Photoconductance measured on the same Corbino sample excited by a linearly polarized MW radiation. The MW amplitude is modulated by a lock-in amplifier. The miniscule photoconductance in the bulk gap demonstrates that the 2D bulk states make no contribution to the photocurrent. (c) Magnetoresistance measurements on a Hall-bar device. The plateau increases with parallel magnetic fields, indicating an enhancement of backscattering under broken TRS. (d) Resistance of the Hall-bar device in (c) measured by fixing the backgate at the plateau and sweeping a parallel magnetic field. A small bias current is used to avoid the heating effect. Resistance doubled at 1 T and showing saturation above 1 T.

measurement in Fig. 1(b) shows that when the Fermi level is tuned inside the bulk gap, the resistance of the Hall-bar sample exhibits a maximum near the CNP, while the Corbino sample experiences a conductance minimum close to zero, indicating negligible bulk contribution. In other words, the dc current flowing through the Hall bar near the CNP is mainly carried by the edge states. A differential photovoltage signal V_{ph}^{f}, which is induced under MW irradiation, is measured from the voltage drop between the two contacts with frequency f locked to the modulation frequency of the MW amplitude. Differential photocurrent I_{ph}^{f} is measured by the photovoltage drop across a load resistor with a resistance R_L that is much smaller than the resistance of the sample itself.

InAs/GaSb DQWs can be modeled by the Bernevig-Hughes-Zhang (BHZ) effective Hamiltonian [4],

$$\mathrm{H} = H_0 + H_{\mathrm{BIA}} + H_{\mathrm{SIA}}, \tag{1}$$

with bulk inversion asymmetry (BIA) term H_{BIA} and structural inversion asymmetry (SIA) H_{SIA} in addition to the quantitative correction due to electron-hole hybridization. Projected to the effective four-band basis, H_{SIA} could be recognized as a k-linear Rashba term (neglecting the high-order k-cubic term) responsible for deviation from spin perfect alignment away from the CNP [18]. Despite these factors, the QSH effect still persists in this system with the help of gate tuning, and resistance quantization can be observed in samples with size smaller than the phase coherent length [7,8,12,13]. For longer samples, the longitudinal resistance is

larger than the quantization value. The increasing resistance under magnetic fields near the CNP [Figs. 2(c) and 2(d)] indicates backscattering enhancement of the edge state since the contribution of the bulk state can be excluded. This can be interpreted as the destroying QSH states by breaking time-reversal symmetry (TRS) [12,13]. Here resistance saturation happens at a smaller field, which is consistent with our previous studies [13], and a small excitation current is used to reduce heating. Theoretically large magnetic fields might also form Landau levels in the bulk ($B_\perp$) or shift the subbands to the semimetal regime ($B_\parallel$). Neither of those effects is relevant to our case here [13]. Except from the truly dc insulating bulk [Fig. 2(a)], we also demonstrate in Fig. 2(b) that when excited by MW radiation, the bulk still contributes no photoconduction up to 8 T, whereas in the Hall-bar sample data shown in Fig. 3 and Fig. 4, nontrivial photocurrent and photovoltage are observed. Therefore, it is reasonable to conclude that the photoresponse signal comes from the sample edges when the Fermi level is tuned in the bulk gap.

Generally, when a semiconductor device is illuminated with MW radiation, charge carriers below the Fermi level absorb photon energy and become mobile within a certain relaxation time. Note that in the MW photoexcitation scenario, interband resonant absorption is not relevant due to energy scale. These mobile charge carriers will drift under a bias electric field induced by external current application. Therefore, the photocurrent formed always has the same polarity with the
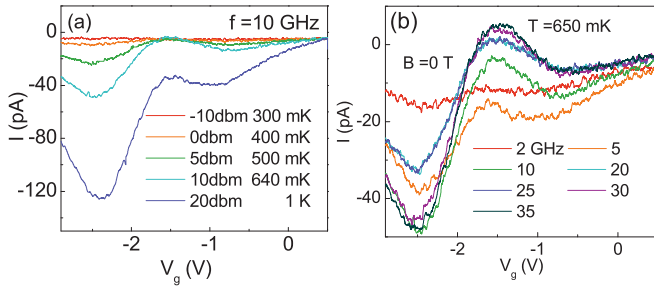
FIG. 3. (a) The MW power-dependent photocurrent traces measured in a Hall-bar device with no magnetic field application and a large external bias current. Enhanced photocurrent on both sides of the gap boundary is detected with increasing MW radiation. Miniscule photocurrent at the CNP is maintained up to 10 mW. This phenomenon starts to break down at 100 mW MW power due to heating. The conventional unit dbm is defined as $P(\text{dbm}) = 10 \log_{10} \frac{P(\text{W})}{1\text{mW}}$, where $P(\text{dbm})/P(\text{W})$ stands for power in the unit of dbm/Watt. (b) MW frequency-dependent photocurrent measurement is shown by tuning the MW power to keep temperature at a fixed value of 650 mK. This is chosen instead of using a fixed MW input power in order to rule out the possibility of different attenuations at various frequency ranges. Shifting of the CNP towards a lower backgate voltage is observed with increasing MW frequency.

external bias [Fig. 4(a)]. However, the voltage drop caused by this mechanism is due to the fact that electrons and holes are spatially separated, meaning the voltage drop always tries to compensate for the external field. As a result, when a negative bias current is applied, the current shows a negative sign while the voltage is positive [Fig. 4(b)]. Note that this case is different from photocurrents excited by circularly polarized radiation in unbiased devices in [15] where spin is selectively excited. It was recently proposed in [18] that unlike in the centrosymmetry model where only magnetodipole interaction is able to couple the spin-up and spin-down branches, for a crystal lack of inversion symmetry, optical transition occurs due to electron-dipole interaction which is several orders of magnitude stronger. In the external-current-dependence
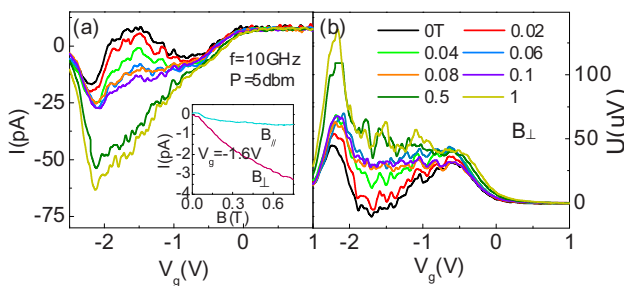

FIG. 4. (a) Photocurrent and (b) photovoltage measurement in a Hall-bar device with fixed MW frequency and power. The back-gate voltage is swept at different perpendicular magnetic fields. A moderate magnetic field is employed to break TRS, thus causing Rashba-type spin flipping between the two branches of the helical edge states. This results in an enhancement of the photocurrent and photovoltage in the bulk gap. Comparison between the effect of parallel and perpendicular magnetic fields is displayed in the inset of (a), indicating a larger *g* factor for perpendicular fields.

measurement, a negligible zero-bias photocurrent shows that the dichroism for circularly polarized light is small for this material.

An optical transition rate can be estimated by first-order perturbation theory, where excited states are

$$|m\rangle \approx |m^0\rangle + \sum_k \frac{H'_{fm}}{E_m^{(0)} - E_k^{(0)}} |k^0\rangle. \qquad (2)$$

Here, $|m^0\rangle/|m\rangle$ is the initial/final state, H'_{fm} is the off-diagonal matrix element for perturbation, and $E_k^{(0)}$ is the energy from solving the nonperturbed equation. The resultant photocurrent is determined by the number of excited carriers and their drift velocity in an external electric field. Given the same microwave power and frequency, the transition rate is set by the density of states (DOS) and perturbation strength H'_{fm} of the initial/final state assuming certain interaction efficiency between electrons and photons. The electric field in the sample equals the bias voltage divided by the distance across the two leads. In the bulk gap where the bulk contribution can be neglected [Fig. 2(a)], the external voltage is effectively applied on the edge state carrier. Therefore, at the resistance peak shown in Fig. 2(c), the effective electric field also has a maximum. However, we observed a photocurrent minimum near the CNP (Fig. 3) which can only be explained via a reduction in transition rate. This is a reasonable result because when the Fermi level is positioned in the conduction and valence bands, there is only one mode available: the linearly dispersed edge state. This results in a reduction of DOS for both the initial and final states since the microwave photons have an energy level of a few tens of μeV, which is much smaller than the bulk gap. Also note that due to the helical nature of the edge states, two states at a fixed k have partially opposite spin (taking the H_{BIA} and H_{SIA} terms into account) [17], so the transition rate between two states with the same momentum is further reduced because of a reduction in H'_{fm}. Momentum conservation is another reason to constrain this transition because the momentum transferred in an electron-photon interaction can usually be neglected. Here data are collected by repeatedly downwards sweeping gate voltage to rule out a hysteresis effect due to charge relaxation in the gate.

When we increase the microwave power, the data in Fig. 3(a) show that the photocurrent increases with MW radiation until heating comes into play where thermal energy might also start to excite carriers. Note that 10 GHz microwave photons have equivalent thermal energy of about 0.5 K. In addition, we tune MW power to fix the temperature at 650 mK in order to rule out the attenuation effect in the circuit and vary MW frequency. Except from frequencies below 5 GHz where photon energy is much lower than thermal energy (heating effect dominates), no frequency dependence is observed up to 40 GHz [Fig. 3(b)]. We attribute this phenomenon to the lack of clear absorption edge in the band structure in this system. Interestingly, there is a large voltage shift ($\sim$0.1 V) of the photocurrent minima around three orders of magnitude larger than the MW photon energy which known mechanisms do not explain.

Theoretically, the application of magnetic field opens a gap on the edge state dispersion near the CNP [17,19]. However, the observation of this gap is extremely difficult

in this disordered system where fluctuations provided by the randomly positioned scattering centers should be considered; for instance, the bulk inhomogeneities near the edge induced by the ionized dopant atoms in the QW, disordered nuclear spins [20], or the charge puddles [21,22] formed in the bulk. The resultant band structure might be locally shifted, making the observation of the gap opening in the edge state by a magnetic field very difficult.

However, we find that for a fixed microwave frequency, the application of either perpendicular or parallel magnetic field increases both the photocurrent and photovoltage (Fig. 4) saturating at the value where dc resistance saturates as well. We attribute this phenomenon to the same TRS broken process that induces backscattering, which may provide some momentum transferring in the electron-photon interaction. Note that the photocurrent signals also show saturation behaviors under a small magnetic field, similar to the measured resistance [Figs. 2(c) and 2(d)]. It is found that a perpendicular magnetic

field has a larger effect than a parallel field [Fig. 4(a) inset], indicating a larger out-of-plane g factor. The same situation holds for radiation where the electric field is either along or perpendicular to the edge, which is consistent with the particle-hole symmetry-broken case in real semiconductor structures [18].

In conclusion, we have studied the photoresponse of edge states in InAs/GaInSb DQWs biased by external electric field under microwave radiation. We demonstrate that the photocurrent purely comes from the edge state, while bulk makes no contribution in the gap. The frequency, temperature, and magnetic field dependence of the photoresponse further explore the nature of edge state in this system, which we properly model with QSH physics.

[1] C. L. Kane and E. J. Mele, Phys. Rev. Lett. **95**, 226801 (2005).

[2] C. L. Kane and E. J. Mele, Phys. Rev. Lett. **95**, 146802 (2005).

[3] X.-L. Qi and S.-C. Zhang, Rev. Mod. Phys. **83**, 1057 (2011).

[4] C. Liu, T.-L. Hughes, X.-L. Qi, K. Wang, and S.-C. Zhang, Phys. Rev. Lett. **100**, 236601 (2008).

[5] I. Knez, R.-R. Du, and G. Sullivan, Phys. Rev. Lett. **107**, 136603 (2011).

[6] I. Knez, C. T. Rettner, S.-H. Yang, S. S. P. Parkin, L. Du, R.-R. Du, and G. Sullivan, Phys. Rev. Lett. **112**, 026602 (2014).

[7] L. Du, X. Li, W. Lou, G. Sullivan, K. Chang, J. Kono, and R.-R. Du, Nat. Commun. **8**, 1971 (2017).

[8] T. Li, P. Wang, H. Fu, L. Du, K. A. Schreiber, X. Mu, X. Liu, G. Sullivan, G. A. Csáthy, X. Lin, and R.-R. Du, Phys. Rev. Lett. **115**, 136804 (2015).

[9] S. Mueller, C. Mittag, T. Tschirky, C. Charpentier, W. Wegscheider, K. Ensslin, and T. Ihn, Phys. Rev. B **96**, 075406 (2017).

[10] B.-M. Nguyen, A. A. Kiselev, R. Noah, W. Yi, F. Qu, A. J. A. Beukman, F. K. de Vries, J. van Veen, S. Nadj-Perge, L. P. Kouwenhoven, M. Kjaergaard, H. J. Suominen, F. Nichele, C. M. Marcus, M. J. Manfra, and M. Sokolich, Phys. Rev. Lett. **117**, 077701 (2016).

[11] T. Akiho, F. Couëdo, H. Irie, K. Suzuki, K. Onomitsu, and K. Muraki, Appl. Phys. Lett. **109**, 192105 (2016).

[12] L. Du, T. Li, W. Lou, X. Wu, X. Liu, Z. Han, C. Zhang, G. Sullivan, A. Ikhlassi, K. Chang, and R.-R. Du, Phys. Rev. Lett. **119**, 056803 (2017).

[13] T. Li, P. Wang, G. Sullivan, X. Lin, and R. R. Du, Phys. Rev. B **96**, 241406(R) (2017).

[14] G. C. Dyer, X. Shi, B. V. Olson, S. D. Hawkins, J. F. Klem, E. A. Shaner, and W. Pan, Appl. Phys. Lett. **108**, 013106 (2016).

[15] K.-M. Dantscher, D. A. Kozlov, M. T. Scherr, S. Gebert, J. Bärenfänger, M. V. Durnev, S. A. Tarasenko, V. V. Bel'kov, N. N. Mikhailov, S. A. Dvoretsky, Z. D. Kvon, J. Ziegler, D. Weiss, and S. D. Ganichev, Phys. Rev. B **95**, 201103 (2017).

[16] Q. Ma, S.-Y. Xu, C.-K. Chan, C.-L. Zhang, G. Chang, Y. Lin, W. Xie, T. Palacios, H. Lin, S. Jia, P. A. Lee, P. Jarillo-Herrero, and N. Gedik, Nat. Phys. **13**, 842 (2017).

[17] C. P. Orth, G. Strubi, and T. L. Schmidt, Phys. Rev. B **88**, 165315 (2013).

[18] M. V. Durnev and S. A. Tarasenko, arXiv:1805.04331.

[19] J. Maciejko, X. L. Qi, and S. C. Zhang, Phys. Rev. B **82**, 155310 (2010).

[20] A. D. Maestro, T. Hyart, and B. Rosenow, Phys. Rev. B **87**, 165440 (2013).

[21] J. I. Väyrynen, M. Goldstein, and L. I. Glazman, Phys. Rev. Lett. **110**, 216402 (2013).

[22] J. I. Väyrynen, M. Goldstein, Y. Gefen, and L. I. Glazman, Phys. Rev. B **90**, 115309 (2014).